AFRL-RV-PS-
TR-2013-0130

SOLID STATE LI-ION BATTERIES

Sehee Lee

University of Colorado at Boulder
ECME 275
427 UCB
Boulder, CO 80309-0427

23 Oct 2013

Final Report

AIR FORCE RESEARCH LABORATORY
Space Vehicles Directorate
3550 Aberdeen Ave SE
AIR FORCE MATERIEL COMMAND
KIRTLAND AIR FORCE BASE, NM 87117-5776

DTIC COPY
NOTICE AND SIGNATURE PAGE

This report is the result of contracted fundamental research deemed exempt from public affairs security and policy review in accordance with SAF/AQR memorandum dated 10 Dec 08 and AFRL/CA policy clarification memorandum dated 16 Jan 09. This report is available to the general public, including foreign nationals. Copies may be obtained from the Defense Technical Information Center (DTIC) (http://www.dtic.mil).

AFRL-RV-PS-TR-2013-0130 HAS BEEN REVIEWED AND IS APPROVED FOR PUBLICATION IN ACCORDANCE WITH ASSIGNED DISTRIBUTION STATEMENT

//SIGNED//
DAVID CHAPMAN
Program Manager

//SIGNED//
PAUL HAUSGEN
Technical Advisor, Spacecraft Component Technology Branch

//SIGNED//
BENJAMIN M. COOK, Lt Col, USAF
Deputy Chief, Spacecraft Technology Division
Space Vehicles Directorate

REPORT DOCUMENTATION PAGE

Form Approved
OMB No. 0704-0188

1. REPORT DATE *(DD-MM-YYYY)*	**2. REPORT TYPE**	**3. DATES COVERED** *(From - To)*
22-10-2013	Final Report	20 Aug 2012 – 16 Nov 2013

4. TITLE AND SUBTITLE
Solid State Li-ion Batteries

5a. CONTRACT NUMBER
FA9453-12-1-0238

5b. GRANT NUMBER

5c. PROGRAM ELEMENT NUMBER
62601F

6. AUTHOR(S)
Sehee Lee

5d. PROJECT NUMBER
8809

5e. TASK NUMBER
PPM00017647

5f. WORK UNIT NUMBER
EF008962

7. PERFORMING ORGANIZATION NAME(S) AND ADDRESS(ES)
University of Colorado at Boulder
ECME 275
427 UCB
Boulder, CO 80309-0427

8. PERFORMING ORGANIZATION REPORT NUMBER

9. SPONSORING / MONITORING AGENCY NAME(S) AND ADDRESS(ES)
Air Force Research Laboratory
Space Vehicles Directorate
3550 Aberdeen Ave SE
Kirtland AFB, NM 87117-5776

10. SPONSOR/MONITOR'S ACRONYM(S)
AFRL/RVSV

11. SPONSOR/MONITOR'S REPORT NUMBER(S)
AFRL-RV-PS-TR-2013-0130

12. DISTRIBUTION / AVAILABILITY STATEMENT
Approved for public release; distribution is unlimited.

13. SUPPLEMENTARY NOTES

14. ABSTRACT
Over the last one year, we have worked on an all-solid-state Li-ion battery and demonstrated a specific energy of 225 mWh g^{-1} based upon the combined mass of both the composite anode and cathode. To realize this full cell, we pair an iron sulfide and sulfur composite cathode with a Si-based anode. The anode active material is a Si-Ti-Ni alloy with good ionic and electronic conductivity that attains a stable specific capacity of 400 mAh g^{-1} based upon the total mass of the composite anode. To our knowledge, this is the highest stable Si-based all-solid-state anode specific capacity reported to date. To utilize both a lithium free anode and cathode, we adopt a pre-lithiation technique involving stabilized lithium metal powder. This is the first time that this technique has been demonstrated in an all-solid-state battery.

15. SUBJECT TERMS
Li-ion, solid state, batteries, pyrite, FeS2, specific energy

16. SECURITY CLASSIFICATION OF:			**17. LIMITATION OF ABSTRACT**	**18. NUMBER OF PAGES**	**19a. NAME OF RESPONSIBLE PERSON**
a. REPORT	**b. ABSTRACT**	**c. THIS PAGE**			David Chapman
U	U	U	Unlimited	24	**19b. TELEPHONE NUMBER** *(include area code)*

(This page intentionally left blank)

TABLE OF CONTENTS

LIST OF FIGURES

ACKNOWLEDGMENTS

This material is based on research sponsored by Air Force Research Laboratory under agreement number FA9453-12-1-0238. The U.S. Government is authorized to reproduce and distribute reprints for Governmental purposes notwithstanding any copyright notation thereon.

DISCLAIMER

The views and conclusions contained herein are those of the authors and should not be interpreted as necessarily representing the official policies or endorsements, either expressed or implied, of Air Force Research Laboratory or the U.S. Government.

(This page intentionally left blank)

1 SUMMARY

Over the last one year, we have worked on an all-solid-state Li-ion battery and demonstrated a specific energy of 225 mWh g^{-1} based upon the combined mass of both the composite anode and cathode. To realize this full cell, we pair an iron sulfide and sulfur composite cathode with a Si-based anode. The anode active material is a Si-Ti-Ni alloy with good ionic and electronic conductivity that attains a stable specific capacity of 400 mAh g^{-1} based upon the total mass of the composite anode. To our knowledge, this is the highest stable Si-based all-solid-state anode specific capacity reported to date. To utilize both a lithium free anode and cathode, we adopt a pre-lithiation technique involving stabilized lithium metal powder. This is the first time that this technique has been demonstrated in an all-solid-state battery.

2 INTRODUCTION

Bulk all-solid-state batteries made with mechanochemically prepared Li_2S-P_2S_5 glass-ceramic electrolytes (1-3) are a safe alternative to conventional Li-ion batteries because sulfide based glass-ceramic electrolytes are pure ionic conductors, non-volatile, non-flammable, and stable versus lithium metal. However, the use of lithium metal anodes in all-solid-state batteries (ASSBs) is not straightforward because dendritic lithium can penetrate porous cold-compacted glass-ceramic electrolyte separators. To demonstrate this point, an interfacial instability that was observed by a previous study may be better characterized as an internal short (4). To improve cell cycleability and survivability a recent study has demonstrated that the vapor deposition of thin lithium films onto Li_2S-P_2S_5 glass-ceramic solid-state electrolyte (SSE) pellets can improve electrolyte-lithium electrode interfacial contact (5). However, the conservative cycling parameters used in this study preclude making a conclusion on the viability of all-solid-state lithium metal anodes.

To sidestep the difficulties associated with lithium metal anodes, many ASSB studies utilize an InLi alloy (6, 7). Unfortunately, indium is not a practical anode option because of its high cost. Other ASSB studies utilize a variety of anodes like FeS_2 (8, 9), FeS (10), nano-Si (11-13), $Li_4Ti_5O_{12}$ (14-17), graphite (18, 19), $Li_{4.4}Ge_xSi_{1-x}$ (20), α-Fe_2O_3 (21) and Sn-based glasses like SnO-Br_2O_3 (22) or SnS-P_2S_5 (23). FeS_2, FeS, $L_4Ti_5O_{12}$, α-Fe_2O_3, and Sn-based glasses all have average operating voltages that are too high to make them useful as anodes while Ge is too expensive to make $Li_{4.4}Ge_xSi_{1-x}$ alloys practical. FeS_2 has such a high potential that it is better suited as a cathode. Our previous work has shown that FeS_2's full potential will only be realized if it is used as a cathode (24). In that work, a FeS_2 cathode was paired with a lithium metal anode, however, the survivability of the test cells was diminished by the occasional internal short.

Except for the fact that they are lithium free, graphite and Si are ideal anode candidates to be paired with FeS_2 because they have low operating potentials (< 0.5 V vs. Li^+/Li). Unfortunately, the specific capacities of graphite or Si all-solid-state anodes have not achieved acceptably high values. For effective comparison, specific capacities in this paper are often presented with respect to the total composite electrode mass rather than with respect to only active material mass. For clarity, specific capacities based on active material mass are denoted by (active), while specific capacities based on total electrode mass are denoted by (cathode), (anode), or (electrode). Specific capacity or specific energy is denoted by (cathode + anode) when both electrodes of a full cell are considered. Solid-state graphite anodes have been reported with specific capacities of about 200 mAh g^{-1} (electrode) (18), but further improvement is limited by graphite's relatively low theoretical capacity of 372 mAh g^{-1} (active). At room temperature Si has a specific capacity that is an order of magnitude larger than that of graphite's, but Si's insulating nature limits its mass loading in an all-solid-state electrode. The poor solid-solid interfacial contact between SSE particles and active material particles severely hinders ionic transport to Si. For good reversibility and a high degree of Si utilization, all-solid-state Si-based anodes must be composed predominately of electronically conducting diluent and SSE. In our previous studies with Si-based all-solid-state anodes, we studied electrodes with a 1:5:1 weight ratio of Si, SSE, and conducting additive, respectively (11-13). Due to the poor mass loading of Si, these Si-based all-solid-state anodes could only achieve a stable specific capacity not much greater than 200 mAh g^{-1} (electrode).

To increase the active material mass loading of Si-based all-solid-state anodes, it is best to improve the ionic and electronic conductivity of the active material. Our recent development and characterization of a Si-Ti-Ni (STN) ternary alloy for commercial Li-ion cells suggest that this material would be ideally suited as an active material for Si-based all-solid-state anodes (25). The STN alloy has a microstructure of nano-Si particle domains embedded in an electrochemically active $Ti_4Ni_4Si_7$ matrix. During the initial lithiation of the STN alloy, the matrix irreversibly takes up some Li^+ to become a mixed conductor with a composition of approximately $Li_{3.2}Ti_4Ni_4Si_7$ and an ionic conductivity of 2.0×10^{-5} S cm^{-1}. We apply the STN alloy to an all-solid-state battery because the $Li_xTi_4Ni_4Si_7$ matrix provides fast ionic conduction to the embedded nano-Si particles. We report that an all-solid-state STN anode achieves a stable specific capacity of 405 mAh g^{-1} (electrode) which is over double the baseline of 200 mAh g^{-1} (electrode) set by the previously mentioned graphite and Si-based solid-state anodes.

To realize a full cell, we pair our STN composite anode with our previously described iron sulfide and sulfur (FeS + S) cathode (26). The pairing of a lithium free FeS + S cathode and a lithium free STN anode presents an easily overcome obstacle. Our Li_3N decomposition pre-lithiation technique is not appropriate for conversion materials or for anodes with operating voltages less than 0.44 V vs. Li^+/Li (27) so we adopt a lithiation technique utilizing stabilized lithium metal powder (SLMP). Previously, this method had only been demonstrated in conventional liquid cells (28, 29).

3 METHODS, ASSUMPTIONS, AND PROCEDURES

All cell fabrication and testing for this study was carried out under an inert Argon gas environment. The glass electrolyte used in this study is the previously described $77.5Li_2S{:}22.5P_2S_5$ glass SSE (12). The FeS + S cathode was prepared by mechanochemically combining FeS and S precursors with the glass SSE (26). The pre-lithiated Si-Ti-Ni (STN) alloy anode was fabricated in a two- step process. First, STN powder (MK electron, 66 at. % Si, air jet milled) (25), SSE, and carbon black (TimCal, C65) were mixed with an agate mortar and pestle in a ratio of either 7:3:0 or 7:3:2, respectively. Stabilized lithium metal powder (SLMP, FMC Lithium Corp., Lectro Max powder 100) was then combined with the 7:3:2 composition STN anode powder via vortex mixing (Vortex Genie 2) in a weight ratio of 1 to 5.21, respectively.

To measure the electronic conductivity of the STN matrix, $Ti_4Ni_4Si_7$ and $Li_{3.2}Ti_4Ni_4Si_7$ were prepared as described elsewhere (25). A potential sweep was then applied to cold-compacted pellets of $Ti_4Ni_4Si_7$ and $Li_{3.2}Ti_4Ni_4Si_7$ with Ti current collectors. The shell of our all-solid-state batteries is a titanium-polyaryletheretherketone (PEEK) test cell die (Figure 1). To fabricate each cell, the glass SSE powder was compressed to 1 metric ton inside the Ti-PEEK die to form the separator pellet. 5 mg of the FeS + S cathode powder and 8.36 mg of the pre-lithiated STN anode powder were then cold-pressed to opposite sides of the glass electrolyte pellet with 5 metric tons force. All cells were cycled under constant current constant voltage (CCCV) conditions using an Arbin BT2000 battery tester at 60°C. In this report, charge and discharge refer to the lithiation and delithiation of the STN alloy, respectively. Materials were characterized by field emission scanning electron microscopy (FESEM, JEOL JSM-7401F), energy dispersive spectroscopy (EDS) and Cu-Kα X-ray (XRD) measurement.

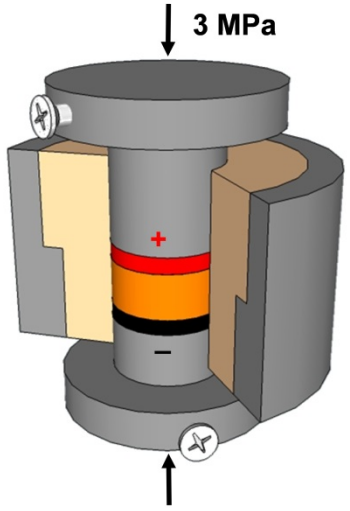

Figure 1. Schematic for our all-solid-state Li-ion battery test dies. The glass electrolyte separator pellet and composite electrodes are cold-pressed sequentially between two Ti plunger-shaped current collectors inside a PEEK-lined Ti die. Cells are cycled under an applied pressure of 3 MPa

4 RESULTS AND DISCUSSION

STN composite electrodes with and without carbon black were electrochemically characterized vs. a lithium counter electrode. Figure 2 presents the cycling data for the 7:3 and 7:3:2 weight ratio composite electrode compositions of STN:SSE and STN:SSE:carbon black, respectively. It was found that the addition of carbon black dramatically improves cell reversibility. The STN electrode with carbon black achieves a 1st cycle discharge (delithiation)

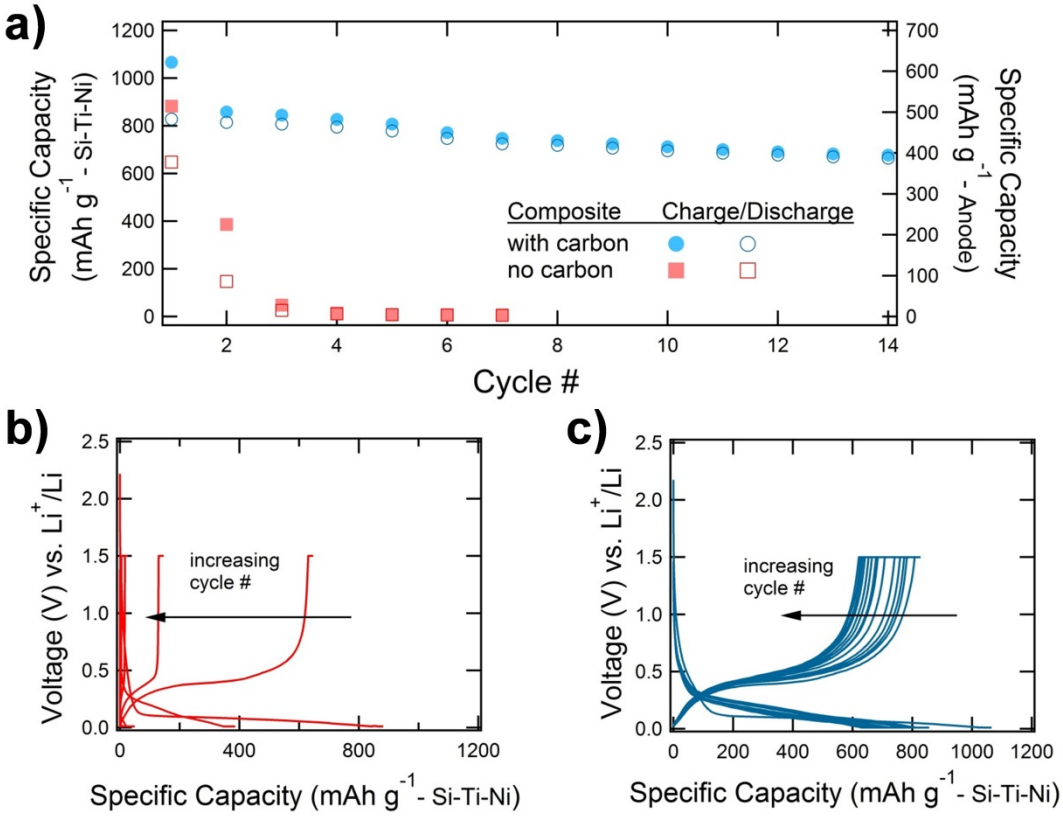

Figure 2. (a) Cyclic stability of STN electrodes without carbon black (red square) and 16.7 weight % carbon black (blue circle). Charge refers to the lithiation of the STN alloy while discharge refers to the delithiation of the STN alloy. (b) Voltage profiles for the STN electrode without carbon black. (c) Voltage profiles for the STN electrode with 16.7 weight % carbon black

specific capacity of 483 mAh g^{-1} (electrode) and a 10th cycle discharge (delithiation) specific capacity of 405 mAh g^{-1} (electrode). These numbers correspond to an active material specific capacity of 828 and 695 mAh g^{-1} (active) for the 1st and 10th cycles, respectively. This same electrode also has a Coulombic efficiency that improves rapidly from 77.7% on the first cycle to 98.2% by the 10th cycle. The cell then failed with an internal short on the 15th cycle and no further data was recorded. Our previous liquid STN half cell exhibited a first cycle Coulombic efficiency of 87.7% (25). The all-solid-state half cell has a lower Coulombic efficiency because

the all-solid-state cell's comparatively larger amount of carbon black may have induced more side reactions during the initial charge cycle.

To explain why the addition of carbon black improves STN's cycleability, the electronic conductivity of the STN matrix was tested before and after lithiation. Ionic conductivities of the STN matrix were previously measured (25). The $Ti_4Ni_4Si_7$ matrix has a negligible ionic conductivity and an electronic conductivity of 10 S cm^{-1}. After electrochemical activation, the $Li_{3.2}Ti_4Ni_4Si_7$ matrix's ionic conductivity increases to 2.0 x 10^{-5} S cm^{-1} but its electronic conductivity decreases two orders of magnitude to 0.24 S cm^{-1}. The decrease in the matrix's electronic conductivity explains why the STN composite electrode without carbon black could achieve a high initial capacity, but suffered from rapid capacity fade in subsequent cycles. Our previous studies with nano-Si required a nano-Si:SSE:conducting additive ratio of 1:5:1 (11, 12). Because the $Li_xTi_4Ni_4Si_7$ matrix is a mixed conductor, the active material to carbon black mass ratio is increased from 1 to 3.5 and the active material to SSE mass ratio is increased from 0.2 to 2.33 over those previous studies.

Figure 3a presents the FESEM characterization of the uncompressed 7:3:2 weight ratio composite electrode powder. From this micrograph, it is evident that the composite electrode is comprised primarily of particles ranging from 1 to 6 microns in diameter. Figure 3b presents the elemental mappings for Si (red) and S (blue) overlaid on the accompanying FESEM micrograph. As expected, elemental mappings of Si and S are largely segregated to separate particles. Si rich particles are identified as STN particles, while S rich particles are identified as SSE particles. It is evident that the size of the STN particles is well matched to that of the sulfide glass SSE particles. Figure 3c presents the elemental mapping of C (green) overlaid on the same FESEM micrograph. We find that the carbon black particles are well dispersed throughout the composite electrode powder for good electronic transport to accommodate the decrease in the STN's electronic conductivity after the first cycle.

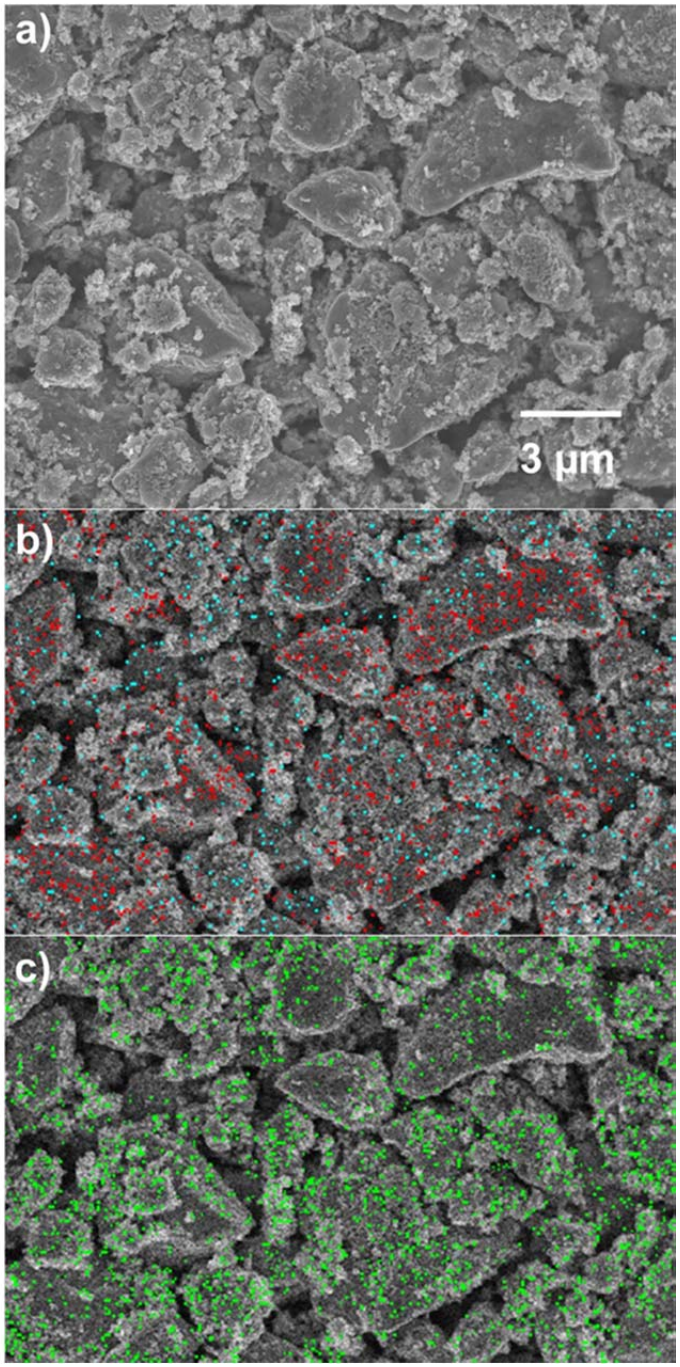

Figure 3. (a) FESEM micrograph of an uncompressed STN electrode. (b) Elemental mappings of Si (red) and S (blue) which demonstrate size compatibility of glass SSE and STN particles. (c) Elemental mapping of C (green) demonstrating good dispersion of carbon black

The next step of this study was to pair the optimized solid-state STN anode with a FeS_2 cathode. As a substitute for FeS_2, we instead utilize a recently developed mechanochemically prepared FeS + S composite active material (26) because all-solid-state electrodes made with this material can achieve higher overall specific capacities. The electrochemical characterization of a all-solid-state FeS + S/Li half cell cycled at 60°C is provided in Figure 4 as a reference to the reader. The FeS + S composite active material has the same theoretical capacity as FeS_2 but can be synthesized much more readily from inexpensive precursors. From Figure 4 it is observed that the capacity of a FeS + S composite electrode quickly exceeds its theoretical value of 900 mAh g^{-1} (active) or 281 mAh g^{-1} (electrode). Excess capacity is provided by the electrochemical activation of inert Li_2S in the $77.5Li_2S{:}22.5P_2S_5$ glass electrolyte component of the composite electrode. The reversible electrochemical utilization of Li_2S in the SSE is facilitated by the good electronic conductivity of FeS as well as by the nano-size of FeS + S particles. The rise, fall, and stabilization of the electrode's capacity is associated with a complex electrochemistry where the reduction of FeS, S, and electrochemically precipitated FeS_2 phases all occur concurrently. After 60 cycles, the FeS + S composite electrode evolves a redox chemistry that is dominated by sulfur.

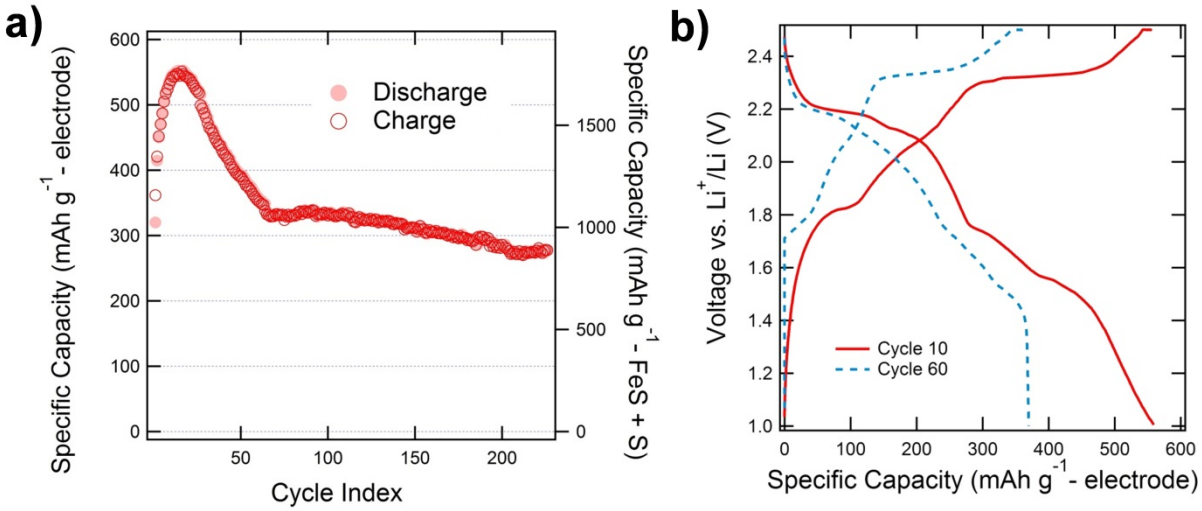

Figure 4. This figure presents the electrochemical characterization of the previously described FeS + S composite electrode (26) which is used as the cathode in this study's full cell demonstration. (a) The cyclic stability of a FeS + S/Li half cell. (b) The 10th and 60th voltage profiles of a FeS + S/Li half cell

We adopted Jarvis et al.'s anode pre-lithiation technique (29) by incorporating SLMP into the uncompressed STN electrode powder (Figure 5a). During the cell's initial discharge the cathode is either lithiated by the direct oxidation of unreacted lithium metal or by the de-alloying of the pre-lithiated STN alloy. During subsequent cycles the cell behaves as a Li-ion battery. The cyclic stability of the FeS + S/STN full cell is given in Figure 5b. The cell achieves a 1st cycle specific discharge of 295 mAh g^{-1} (cathode) which corresponds to a FeS + S specific capacity of 944 mAh g^{-1} (active). This initial discharge capacity is close to the theoretical specific capacity of the FeS + S active material and it is consistent with previous results presented in Figure 4 (26). As expected, the initial specific charge capacity rises dramatically to 383 mAh g^{-1} (cathode)

and the discharge voltage plateaus centered at 1.6V fade with extended cycling. Both of these results are also consistent with prior results. The increase in capacity is attributed to the electrochemical activation of excess Li_2S in the SSE component of the cathode (26, 30) and the fade of the lower voltage plateaus indicates that the sulfur redox chemistry comes to dominate the electrochemistry of the FeS + S cathode. The activation of excess Li_2S also explains why the full cell's initial discharge profile is different from that of subsequent discharge profiles.

From the voltage profiles of this cell (Figure 5c), it is confirmed that the full cell functions as a Li-ion cell and not as a lithium metal cell because the average discharge potential of the full cell is depressed compared to that of a FeS + S half cell (26). The full cell also has a much more stable capacity compared to that of either the individual STN half cell (Figure 2c) or the FeS + S half cell (Figure 4). By the 100^{th} cycle, the full cell maintains a specific discharge capacity of 355 mAh g^{-1} (cathode). When the mass of both composite electrodes are taken into account, the full cell delivers 225 mWh g^{-1} (anode + cathode) upon its 100^{th} discharge.

The FeS + S/Li and STN/Li half cells both behave much differently than the full cell. As discussed, the FeS + S/Li half cell's capacity dramatically rises, falls, and stabilizes, while the 7:3:2 composition STN/Li half cell looses 34% of its capacity between its 1^{st} and 10^{th} charge (lithiation) cycles. The stability of the full cell can be explained by considering three points. First, an excess of SLMP is added to the STN composite anode powder to offset inefficiencies and improve cyclic stability (28). Second, the FeS + S cathode's complex electrochemistry is uniquely capable of offsetting the initial Coulombic inefficiency and fade of Si-based anodes. The characteristic rapid rise of the FeS + S cathode's capacity due to Li_2S activation in the SSE may help to offset losses from the STN anode. The result is a full cell with a stable capacity that does not rapidly rise like the FeS + S/Li half cell or initially fade like the STN/Li half cell. And third, the STN anode in the full cell was not fully utilized. From Figure 5b and c it is evident that the STN anode in the full cell never achieves a specific capacity in excess of 240 mAh g^{-1} (anode). This specific capacity should be revised because the mass of the anode in the full cell now considers the 1.35 mg of SLMP added to pre-lithiate the cell. For this reason, the specific capacity is revised to 286 mAh g^{-1} (anode) for accurate comparison with the 405 mAh g^{-1} (anode) achieved by the 7:3:2 STN/Li half cell during its 10^{th} charge (lithiation). Limiting the depth of Si lithiation has been shown to improve the cyclic stability of other Si-based anodes (31). By not fully utilizing the STN anode the same stabilization of capacity may be observed here as well. Incomplete utilization of the STN anode also suggests that further optimization of the full cell configuration may yield higher overall cell energy densities.

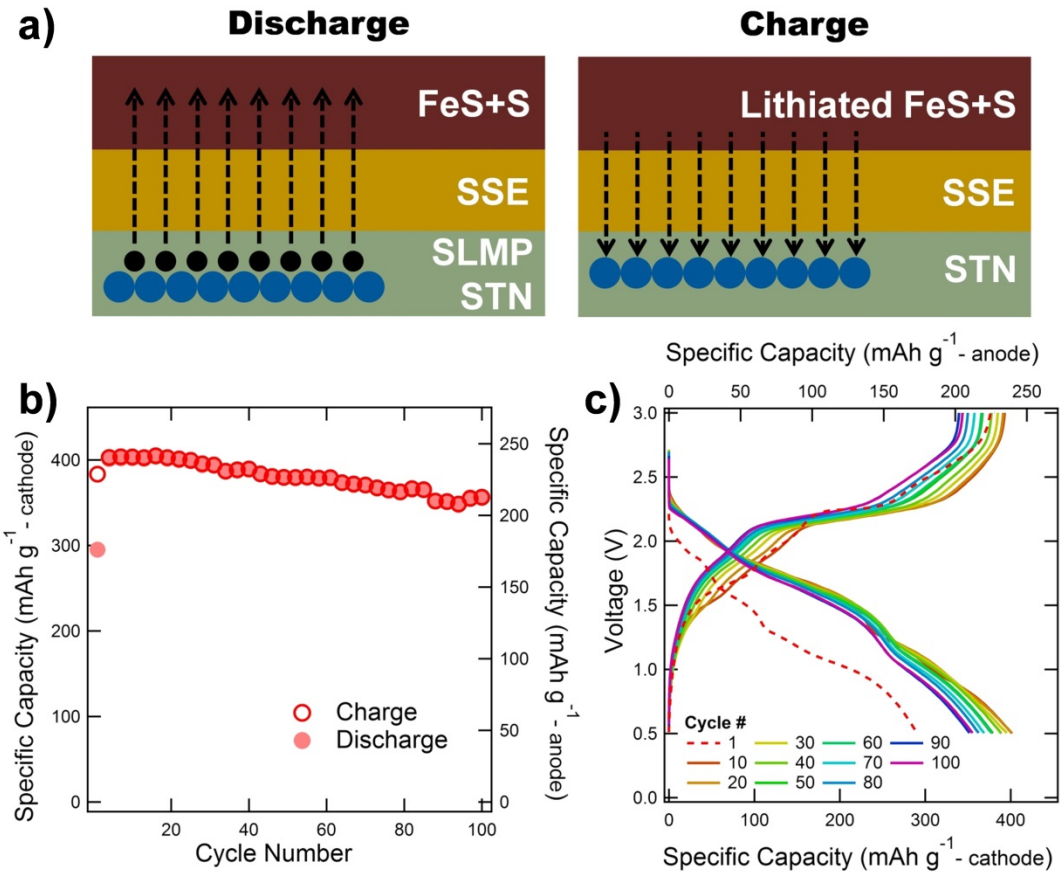

Figure 5. (a) Schematic of the lithiation mechanism. Prior to cell fabrication SLMP is combined with the STN composite anode powder via vortex mixing. (b) Cyclic stability of a full cell with a FeS + S cathode and a pre-lithiated STN anode. (c) Voltage profiles of the same full cell with respect to the mass of the cathode or anode

5 CONCLUSIONS

The Si-Ti-Ni (STN) alloy and Stabilized Lithium Metal Powder (SLMP) pre-lithiation technique were developed with conventional liquid Li-ion batteries in mind, but we find that both are also applicable to all-solid-state Li-ion batteries. STN is well suited as an all-solid-state anode active material because the $Li_xTi_4Ni_4Si_7$ matrix of the STN alloy is a mixed conductor. All-solid-state STN composite anodes provide a stable specific capacity of 400 mAh g^{-1} (anode). For clarity, specific capacities based on active material mass are denoted by (active), while specific capacities based on total electrode mass are denoted by (cathode), (anode), or (electrode). To our knowledge, this is the highest stable Si-based all-solid-state anode specific capacity reported to date. To pre-lithiate an all-solid-state Li-ion battery we incorporated SLMP into the STN composite anode powder prior to cell fabrication. This is the first time that the SLMP pre-lithiation technique has been demonstrated in an all-solid-state battery. By pairing the pre-lithiated STN composite anode with a high capacity FeS + S cathode, an all-solid-state Li-ion battery with a specific energy of 225 mWh g^{-1} (cathode + anode) was demonstrated. The results of this study suggest that all-solid-state batteries can achieve acceptable energy densities without the need for a lithium metal anode. By avoiding the use of lithium metal anodes, the engineering challenges associated with the dendritic penetration of cold-compacted glass solid-state electrolyte (SSE) separators can be circumvented.

REFERENCES

1. A. Hayashi, S. Hama, H. Morimoto, M. Tatsumisago and T. Minami, "High Lithium Ion Conductivity of Glass-Ceramics Derived from Mechanically Milled Glassy Powders," *Chemistry Letters*, **30**, 872 (2001).
2. A. Hayashi, S. Hama, H. Morimoto, M. Tatsumisago and T. Minami, "Preparation of Li_2S-P_2S_5 amorphous solid electrolytes by mechanical milling," *Journal of the American Ceramic Society*, **84**, 477 (2001).
3. M. Tatsumisago, S. Hama, A. Hayashi, H. Morimoto and T. Minami, "New lithium ion conducting glass-ceramics prepared from mechanochemical Li_2S-P_2S_5 glasses," *Solid State Ionics*, **154**, 635 (2002).
4. H. Takahara, M. Tabuchi, T. Takeuchi, H. Kageyama, J. Ide, K. Handa, Y. Kobayashi, Y. Kurisu, S. Kondo and R. Kanno, "Application of lithium metal electrodes to all-solid-state lithium secondary batteries using Li3PO4-Li2S-SiS 2 glass," *Journal of The Electrochemical Society*, **151**, A1309 (2004).
5. M. Nagao, A. Hayashi and M. Tatsumisago, "Fabrication of favorable interface between sulfide solid electrolyte and Li metal electrode for bulk-type solid-state Li/S battery," *Electrochemistry Communications*, **22**, 177 (2012).
6. K. Takada, N. Aotani, K. Iwamoto and S. Kondo, "Solid state lithium battery with oxysulfide glass," *Solid State Ionics*, **86-88**, 877 (1996).
7. N. Kamaya, K. Homma, Y. Yamakawa, M. Hirayama, R. Kanno, M. Yonemura, T. Kamiyama, Y. Kato, S. Hama and K. Kawamoto, "A lithium superionic conductor," *Nature materials*, **10**, 682 (2011).
8. K. Takada, K. Iwamoto and S. Kondo, "Lithium iron sulfide as an electrode material in a solid state lithium battery," *Solid State Ionics*, **117**, 273 (1999).
9. K. Takada, Y. Kitami, T. Inada, A. Kajiyama, M. Kouguchi, S. Kondo, M. Watanabe and M. Tabuchi, "Electrochemical reduction of Li2FeS2 in solid electrolyte," *Journal of The Electrochemical Society*, **148**, A1085 (2001).
10. B.-C. Kim, K. Takada, N. Ohta, Y. Seino, L. Zhang, H. Wada and T. Sasaki, "All solid state Li-ion secondary battery with FeS anode," *Solid State Ionics*, **176**, 2383 (2005).
11. J. E. Trevey, K. W. Rason, C. R. Stoldt and S.-H. Lee, "Improved Performance of All-Solid-State Lithium-Ion Batteries Using Nanosilicon Active Material with Multiwalled-Carbon-Nanotubes as a Conductive Additive," *Electrochemical and Solid-State Letters*, **13**, A154 (2010).
12. J. Trevey, J. S. Jang, Y. S. Jung, C. R. Stoldt and S.-H. Lee, "Glass–ceramic Li2S–P2S5 electrolytes prepared by a single step ball billing process and their application for all-solid-state lithium–ion batteries," *Electrochemistry Communications*, **11**, 1830 (2009).
13. D. M. Piper, T. A. Yersak and S.-H. Lee, "Effect of Compressive Stress on Electrochemical Performance of Silicon Anodes," *Journal of The Electrochemical Society*, **160**, A77 (2013).
14. H. Kitaura, A. Hayashi, K. Tadanaga and M. Tatsumisago, "High-rate performance of all-solid-state lithium secondary batteries using Li4Ti5O12 electrode," *Journal of Power Sources*, **189**, 145 (2009).

15. H. Kitaura, A. Hayashi, K. Tadanaga and M. Tatsumisago, “Electrochemical Analysis of Li4Ti5O12 Electrode in All-Solid-State Lithium Secondary Batteries,” *Journal of The Electrochemical Society*, **156**, A114 (2009).
16. H. Kitaura, A. Hayashi, T. Ohtomo, S. Hama and M. Tatsumisago, “Fabrication of electrode–electrolyte interfaces in all-solid-state rechargeable lithium batteries by using a supercooled liquid state of the glassy electrolytes,” *J. Mater. Chem.*, **21**, 118 (2010).
17. L. Sun, N. Karanjgaokar, K. Sun, I. Chasiotis, W. C. Carter and S. Dillon, “High-strength all-solid lithium ion electrodes based on Li4Ti5O12,” *Journal of Power Sources*, **196**, 6507 (2011).
18. K. Takada, T. Inada, A. Kajiyama, H. Sasaki, S. Kondo, M. Watanabe, M. Murayama and R. Kanno, “Solid-state lithium battery with graphite anode,” *Solid State Ionics*, **158**, 269 (2003).
19. Y. Seino, K. Takada, B.-C. Kim, L. Zhang, N. Ohta, H. Wada, M. Osada and T. Sasaki, “Synthesis of phosphorous sulfide solid electrolyte and all-solid-state lithium batteries with graphite electrode,” *Solid State Ionics*, **176**, 2389 (2005).
20. Y. Hashimoto, N. Machida and T. Shigematsu, “Preparation of Li4.4GexSi1−x alloys by mechanical milling process and their properties as anode materials in all-solid-state lithium batteries,” *Solid State Ionics*, **175**, 177 (2004).
21. H. Kitaura, K. Takahashi, F. Mizuno, A. Hayashi, K. Tadanaga and M. Tatsumisago, “Preparation of α-Fe2O3 Electrode Materials via Solution Process and Their Electrochemical Properties in All-Solid-State Lithium Batteries,” *Journal of The Electrochemical Society*, **154**, A725 (2007).
22. A. Hayashi, M. Nakai, M. Tatsumisago, T. Minami and M. Katada, “Structural Studies in Lithium Insertion into SnO - B 2 O 3 Glasses and Their Applications for All-Solid-State Batteries,” *Journal of The Electrochemical Society*, **150**, A582 (2003).
23. A. Hayashi, T. Konishi, K. Tadanaga, T. Minami and M. Tatsumisago, “All-solid-state lithium secondary batteries with SnS–P2S5 negative electrodes and Li2S–P2S5 solid electrolytes,” *Journal of Power Sources*, **146**, 496 (2005).
24. T. A. Yersak, H. A. Macpherson, S. C. Kim, V.-D. Le, C. S. Kang, S.-B. Son, Y.-H. Kim, J. E. Trevey, K. H. Oh, C. Stoldt and S.-H. Lee, “Solid State Enabled Reversible Four Electron Storage,” *Advanced Energy Materials*, **3**, 120 (2013).
25. S.-B. Son, S. C. Kim, C. S. Kang, T. A. Yersak, Y.-C. Kim, C.-G. Lee, S.-H. Moon, J. S. Cho, J.-T. Moon, K. H. Oh and S.-H. Lee, “A Highly Reversible Nano-Si Anode Enabled by Mechanical Confinement in an Electrochemically Activated LixTi4Ni4Si7 Matrix,” *Advanced Energy Materials*, **2**, 1226 (2012).
26. T. A. Yersak, C. Stoldt and S.-H. Lee, “Electrochemical Evolution of an Iron Sulfide and Sulfur Based Cathode for All-Solid-State Li-Ion Batteries,” *Journal of The Electrochemical Society*, **160**, A1009 (2013).
27. T. A. Yersak, Y. Yan, C. Stoldt and S.-H. Lee, “Ambient Temperature and Pressure Mechanochemical Preparation of Nano-LiTiS2,” *ECS Electrochemistry Letters*, **1**, A21 (2012).
28. C. R. Jarvis, M. J. Lain, Y. Gao and M. Yakovleva, “A lithium ion cell containing a non-lithiated cathode,” *Journal of Power Sources*, **146**, 331 (2005).
29. C. R. Jarvis, M. J. Lain, M. V. Yakovleva and Y. Gao, “A prelithiated carbon anode for lithium-ion battery applications,” *Journal of Power Sources*, **162**, 800 (2006).

30. A. Hayashi, R. Ohtsubo, M. Nagao and M. Tatsumisago, “Characterization of Li2S–P2S5–Cu composite electrode for all-solid-state lithium secondary batteries,” *Journal of Materials Science*, **45**, 377 (2010).
31. U. Kasavajjula, C. Wang and A. J. Appleby, “Nano- and bulk-silicon-based insertion anodes for lithium-ion secondary cells,” *Journal of Power Sources*, **163**, 1003 (2007).

LIST OF SYMBOLS, ABBREVIATIONS, AND ACRONYMS

ASSB	all-solid-state battery
CCCV	constant current constant voltage
EDS	energy dispersive spectroscopy
FESEM	field emission scanning electron microscopy
PEEK	Polyaryletheretherketone
SLMP	stabilized lithium metal powder
SSE	solid-state electrolytes
STN	Si-Ti-Ni
XRD	X-ray diffraction

DISTRIBUTION LIST

DTIC/OCP
8725 John J. Kingman Rd, Suite 0944
Ft Belvoir, VA 22060-6218 1 cy

AFRL/RVIL
Kirtland AFB, NM 87117-5776 2 cys

Official Record Copy
AFRL/RVSV/David Chapman 1 cy